LONG-TERM DETERIORATION OF QUASI-ACTUAL SCALE PRESTRESSED CONCRETE BEAM DUE TO ALKALI-SILICA REACTION

Takanobu Yokoyama*[1], Toyo Miyagawa[2], Yukio Hiroi[3], Takashi Yamamoto[4], Hideki Manabe[5], Takashi Ookubo[6]

[1]Technology and Construction Section, Nippon PS Co., Ltd., Osaka, JAPAN

[2]Infra-System Management Research Unit, Kyoto University, Kyoto, JAPAN

[3]Engineering Department, PC Division, IHI Construction Service Co., Ltd., Osaka, JAPAN

[4]Department of Civil & Earth Resources Engineering, Kyoto University, Kyoto, JAPAN

[5]CORE Institute of Technology Corporation, Osaka, JAPAN

[6]Engineering Section, Business Promotion Dapartment, Kawada Construction Co., Ltd., Osaka, JAPAN

Abstract

Degree of deterioration by alkali-silica reaction (ASR) varies between structures or between members or locations of a structure, depending on environmental or confinement conditions. Mechanical performance of concrete structures depends on the mechanical properties of concrete and reinforcing bars as well as those of the bond between them. In order to ensure safety of a structure damaged by ASR which affects mechanical properties of concrete, the degree of deterioration should be accurately determined for proper quantitative evaluation of the mechanical performance of the structure. This study consisted of long-term exposure and measurement followed by a loading test using unprecedentedly large-size prestressed concrete (PC) beam specimens simulating real PC structures affected by ASR. Control specimens were also prepared for comparison and subjected to the loading test. This paper reports results of the study and the visual observation of the cut sections of the specimens after the loading test.

Keywords: post-tensioned prestressed concrete beam, quasi-actual scale, long-term exposure test, static loading test, visual observation of the cut section

1 LONG-TERM MEASUREMENT USING SPECIMENS UNDER ASR EXPOSURE

1.1 Outline of the specimens

Long-term measurement under exposure to alkali-silica reaction (ASR) was conducted by Japan Prestressed Concrete Contractors Association, using large- and medium-size concrete beam specimens containing alkali-silica reactive or non-reactive aggregate (four specimens in total).

The large specimens had a cross-sectional area equivalent to or larger than that of a post-tensioned prestressed concrete (PC) simple T-girder bridge, and the medium specimens had a cross-sectional area equivalent to or larger than that of a pre-tensioned PC simple T-girder bridge. Prestress was applied by using the post-tensioning system to create stress states where axial compressive stress (P/A) was similar to those in real structures. Longitudinal profile of prestressing bars has a significant influence on the eccentric moment due to the prestress as well as the vertical component of force due to the bending-up of the bars. Since the purpose of this study was to identify the basic behaviors of ASR-affected structures, the prestressing bars were laid straight at the center of the cross section to eliminate eccentric moment and vertical component of force and simplify the effects on ASR deterioration or load carrying behavior.

The control and ASR specimens were manufactured to the same dimensions and same structure in February 2005 [1], and subjected to about 7.5 years of external exposure to allow for ASR deterioration until August 2012 when the bending fracture test was conducted. Figure 1 shows the dimensions of the specimens and the layout of the reinforcing and prestressing bars.

1.2 Crack measurement results

Figure 2 shows changes in crack density of the ASR specimens during 7.5 years after the manufacture. Crack density increased with age, showing a progress of ASR deterioration. Figure 3 shows crack density with

* Correspondence to: t.yokoyama@nipponps.co.jp

respect to the crack width. The ratios of wider cracks to the total increased with age. The measurements were conducted basically during spring or autumn seasons, except for the last measurement which was conducted in July (summer) immediately before the loading test. This explains the significant increases found in the last measurement, and the general trend can be considered to be toward a convergence.

The crack density used in this study is the product of crack length and crack width per unit area (Method B), not the commonly-used total crack length per unit area (Method A). The purpose of using Method B was to take into account the fact that the increase in crack width was more significant than that in crack length after an age of about 500 days [1]. Accordingly, crack density before the fracture test was 5 m•mm/m^2, with obvious increases in both the number and width of the cracks. Figure 4 shows a sketch drawing of cracks observed in the large specimen before the loading test.

1.3 Concrete internal strain measurement results

Concrete internal strain was measured by using the concrete strain gauge (KM-100BT; gauge length: 100 mm) and reinforcing steel strain gauge installed in the central part of the specimens. Figures 5 and 6 show the internal strain measurement results of the medium and large specimens, respectively. Increase in strain was faster in the large specimen than in the medium specimen, which was likely attributable to the effect of the size difference between the specimens (volume effect). Internal strain in the large specimen was found to be 6500×10^{-6} in the transverse direction or 3500×10^{-6} in the vertical direction at the final measurement.

1.4 Ultrasonic propagation velocity measurement results

Figure 7 shows changes in ultrasonic propagation velocity in each specimen. The measurement was taken for two cases with incident waves applied from two sides of the specimen or from the top and bottom of the specimen. Ultrasonic propagation velocity decreased to about 3300 m/s by the last measurement in the ASR specimens of both sizes. All specimens showed a similar tendency at 2500 days where the values slightly increased. This was first considered to be due to gels or other byproducts filling the cracks. However, the values were found to be low again at the measurement immediately before the loading test. Consequently, it was concluded that the cracks were opened wider during the last measurement due to the high temperatures.

1.5 Relationships between ultrasonic propagation velocity and measurement factors

It is known that there is a high correlation between ASR deterioration and decrease in ultrasonic propagation velocity. This section studies the relationship between the non-destructively obtained ultrasonic propagation velocity and two measurement factors of ASR deterioration: crack density and internal strain.

Relationship between ultrasonic propagation velocity and crack density

Figure 8 shows the relationship between ultrasonic propagation velocity and crack density in the large ASR specimen. Propagation velocity decreased to around 3800 m/s when crack density increased to 1 m•mm/m^2 in both the side-to-side and vertical incidence cases.

Figure 9 shows the relationship between ultrasonic propagation velocity and crack density in the medium ASR specimen. Difference was found in the shape of the curves between crack widths $w \geq 0.05$ mm and $w \geq 0.20$ mm. For $w \geq 0.05$ mm, crack density was about 2.5 m•mm/m^2 when propagation velocity decreased to about 3800 m/s which was reached at a crack density of 1 m•mm/m^2 in the large specimen. Although some measurement errors might be present, these results demonstrate the effect of the specimen sizes, showing more rapid decreases in propagation velocity at lower crack densities in the large specimen.

Relationship between ultrasonic propagation velocity and internal strain

Figure 10 shows the relationship between ultrasonic propagation velocity and internal strain in the large ASR specimen. Although there were minor differences between the side-to-side and vertical incidence cases, propagation velocity decreased to around 3600 m/s when concrete internal strain increased to around 2000×10^{-6}. Internal strain increased with the progress of ASR deterioration, while propagation velocity showed a convergence at around 3500 m/s. However, the measurement immediately before the loading test showed a decrease in propagation velocity and an increase in strain. This behavior which was similar to that found in crack density was considered to be due to the high temperatures during the last measurement.

Figure 11 shows the relationship between ultrasonic propagation velocity and internal strain in the medium ASR specimens. With some differences found between the side-to-side and vertical incidence cases, propagation velocity decreased to around 3400 m/s when concrete internal strain increased to around 2000×10^{-6}. Despite the general tendencies of increase in internal strain with the progress of ASR deterioration and convergence in propagation velocity at around 3500 m/s, the decrease in propagation

velocity and increase in strain were found at the measurement immediately before the loading test, suggesting the effect of the high temperatures.

2 LOADING TEST

2.1 Fracture test for flexural capacity calculation

A loading test was carried out at 22 months when ASR deterioration became significant, under the conditions equivalent to the flexural cracking load assuming the service state. A bending fracture test was carried out at 90 months to compare the flexural capacity between the ASR and control specimens (Figure 12). The following sections describe the bending fracture test at 90 months.

The authors monitored the effects of the existing ASR cracks in the specimens on the flexural failure behavior during the fracture test. The specimens were cut using a wire saw after the test, and internal deterioration and crack development were examined. Test pieces (200 mm in length, 100 mm in diameter) were taken from the cut specimens using a core boring machine, and mechanical properties of the specimens were examined.

The mechanical properties of the core samples are reported in the other paper from the same study [4].

2.2 Results of the fracture test for flexural capacity calculation

Table 1 shows a comparison of flexural failure load of the ASR and control specimens. The mechanical property values used in the calculation of the capacity (fracture resistance moment based on the Design specifications for highway bridges and commentary by Japan Road Association [3]) were the actual measured values of the test pieces. Decrease in capacity was expected in the ASR specimens which had numerous wide cracks and a crack density of 5 m•mm/m^2 by Method B. However, no significant difference was found in the measured flexural capacity between the ASR and control specimens. The measured values were mostly consistent with the calculated values not only in the control specimens but also in the ASR specimens, with the measurement/calculation ratio being 1.04. The use of actual mechanical property values of the test pieces provided accurate calculation of flexural capacity of the ASR-affected structures. All specimens failed in flexural compression mode.

Figure 13 shows the load-displacement curves for the large specimens with a schematic of the loading steps of the test, and Figure 14 shows sketch drawings from the flexural crack observation. According to the visual observation, flexural cracks occurred at a lower load level in the ASR specimen as compared to the control specimen. The control specimen had an obvious point of decrease in stiffness at the initiation of flexural cracks. In contrast, the ASR specimen which already had numerous cracks before the loading test showed a constant decrease in stiffness, without an obvious point of decrease. The control/ASR ratio in vertical displacement at the midspan under the flexural cracking load or below was 0.68 due to the decrease in bending stiffness.

The flexural crack observation revealed that the cracks in the ASR specimens were small in both spacing and width, and were distributed in a wide range in the longitudinal direction.

2.3 Visual observation of internal cracks in the cut section

Figure 15 shows a cut section (at the 1/4 span point from the support) of the large ASR specimen after the fracture test. Although many ASR cracks occurred in the surface regions of the specimen, most of them were found outside the stirrup, with almost no further development into the inside.

3 DISCUSSION

Figure 16 shows load-displacement curves under the maximum load. Changes in gradient were less significant in the ASR specimens than in the control specimens. This was considered to be due to the higher dispersion of flexural cracks in the ASR specimens (Figure 14) which should have resulted in a relatively slower decrease in stiffness.

Figure 17 shows changes in neutral axis which was determined from the strain distribution in the prestressing bars at each loading step. Neutral axes of the large ASR specimen were at lower positions than those of the control specimen at all loading steps. There were two likely reasons for this. One was that, while flexural cracks occurring in the control specimen were small in number and developed quickly upward with the increase in the load, flexural cracks in the ASR specimen were induced by the existing vertical cracks occurring in the cover concrete at the bottom fiber, which resulted in a higher crack dispersion and smaller widths of individual cracks. The other was that the development of flexural cracks was slow as being partly discontinued by the presence of horizontal cracks in the cover concrete (Figure 18).

Although numerous cracks occurred in the ASR specimens in this study, there was no rupture of stirrups or other reinforcing bars. Consequently, it could be concluded that confinement remained effective inside the stirrups to suppress inward development of the cracks.

4 REFERENCES

[1] Japan Society of Civil Engineers (2005): State-of-the-art report on the countermeasures for damage due to alkali-silica reaction – Rupture of reinforcing bars. Concrete Library (124). (in Japanese).

[2] Japan Prestressed Concrete Contractors Association (2009): Experimental study on the properties of prestressed concrete specimen affected by ASR reported by ASR Countermeasure Study Committee in Japan Prestressed Concrete Contractors Association. (in Japanese).

[3] Japan Road Association (2013): Design specifications for highway bridges and commentary. (in Japanese).

[4] Hiroi, Y, Yamamoto, T, Toda, Y, Manabe, H, and Miyagawa, T (to be printed): Experimental and analytical studies on flexural behavior of post-tensioned concrete beam specimen deteriorated by alkali-silica reaction (ASR). 15th ICAAR Proceedings, July 3-7, 2016, São Paulo, Brazil.

TABLE 1: Comparison of flexural failure load.							
			Large specimens		Medium specimens		Remarks
			Control	ASR	Control	ASR	
At initiation of cracks	Calculated	Flexural moment Mc (kN•m)	2942	2782	237	245	
		Load Pc (kN)	1883	1781	345	356	
	Measured	Load Pc' (kN)	1700	1300	380	380	
	Ratio	Pc'/Pc	0.90	0.73	1.10	1.07	
At initial yielding	Calculated	Flexural moment My0 (kN•m)	5909	5778	472	501	
		Load Py0 (kN)	3782	3698	687	729	
		Neutral axis X (m)	0.389	0.490	0.161	0.197	Reference values
At flexural failure	Calculated	Flexural moment Mu (kN•m)	7954	7321	660	631	
		Load Pu (kN)	5090	4686	960	918	
		Neutral axis X (m)	0.244	0.334	0.108	0.135	Reference values
	Measured	Flexural failure load Pu' (kN)	4908	4885	955	1020	
	Ratio	Pu'/Pu	0.96	1.04	0.99	1.11	
Mode of failure			Flexural compression mode	Flexural compression mode	Flexural compression mode	Flexural compression mode	

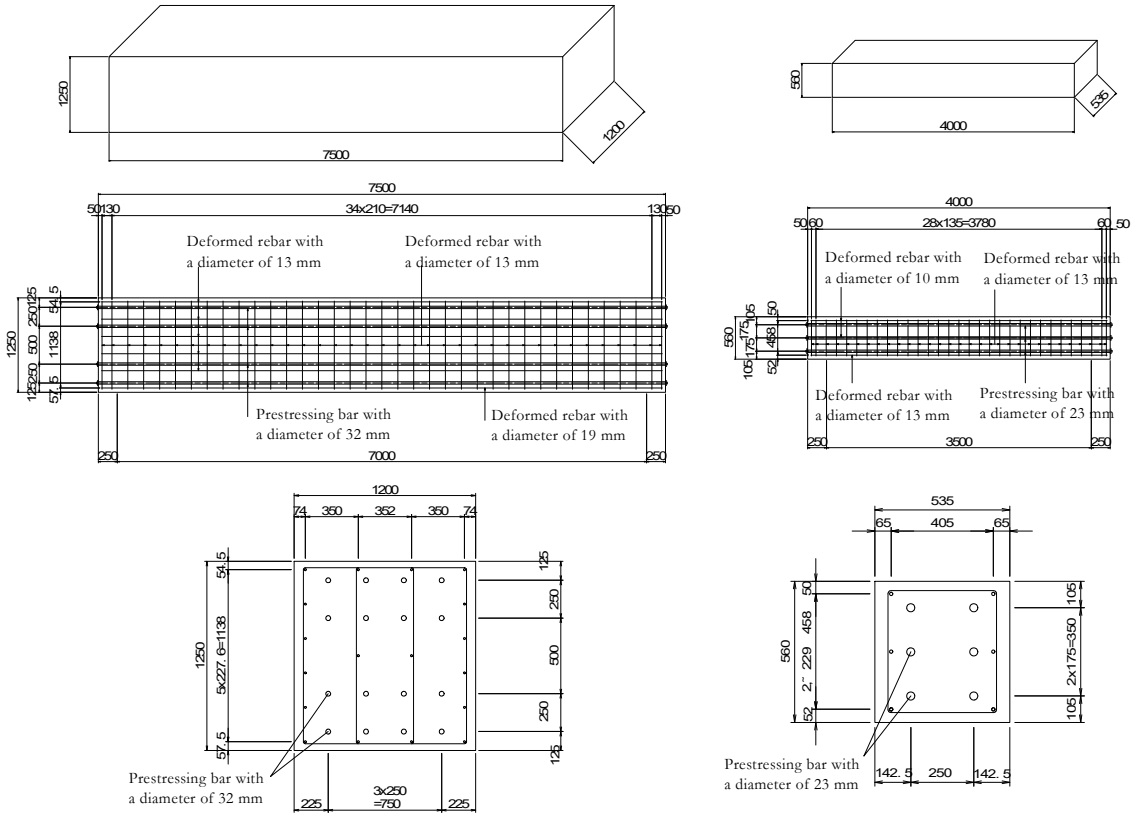

FIGURE 1: Outline of the specimens

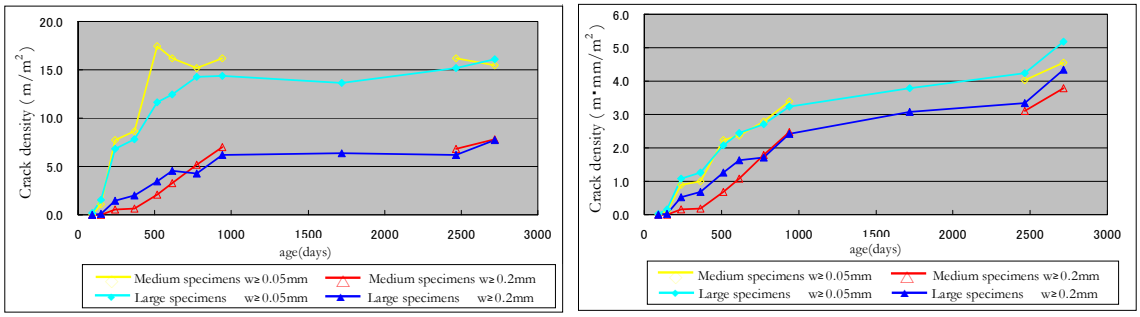

Crack density (m/m²) by Method A Crack density (m•mm/m²) by Method B

FIGURE 2: Changes in crack density

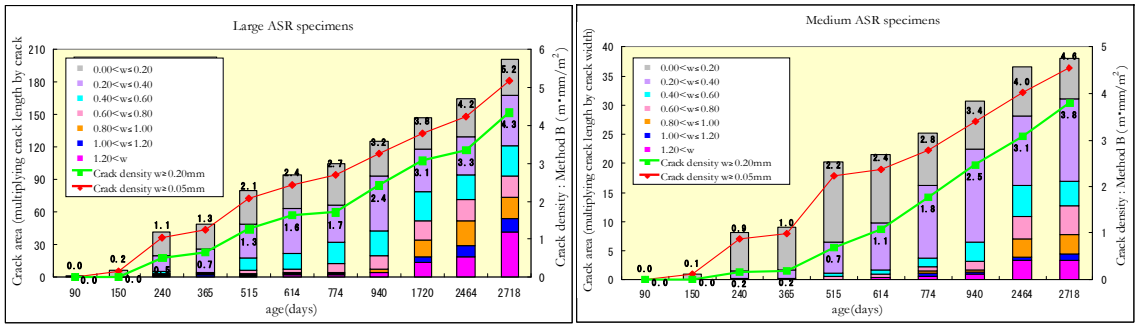

FIGURE 3: Crack density with respect to the crack width

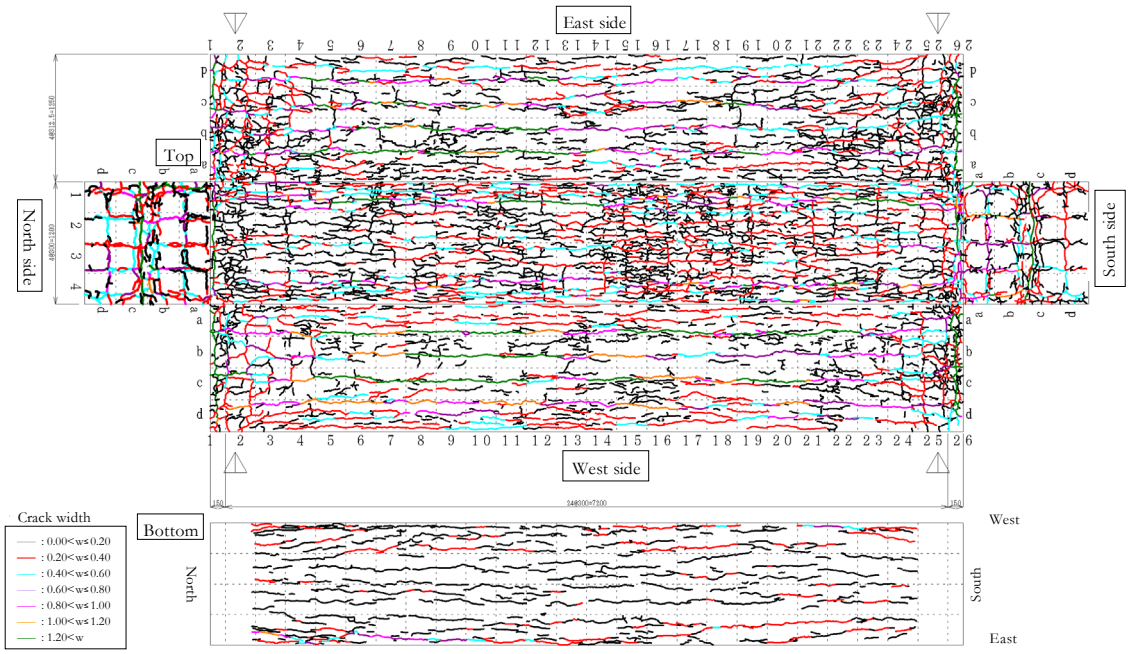

FIGURE 4: Sketch drawing of cracks observed in the large ASR specimen before the loading test

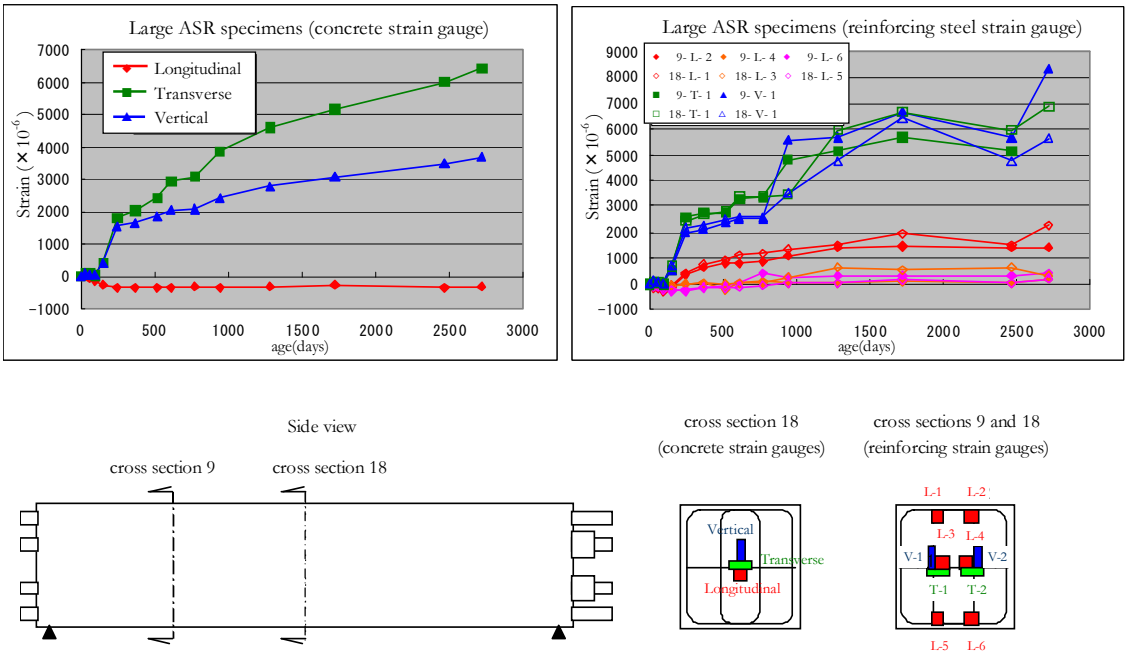

FIGURE 5: Changes in concrete internal strain in the large ASR specimen

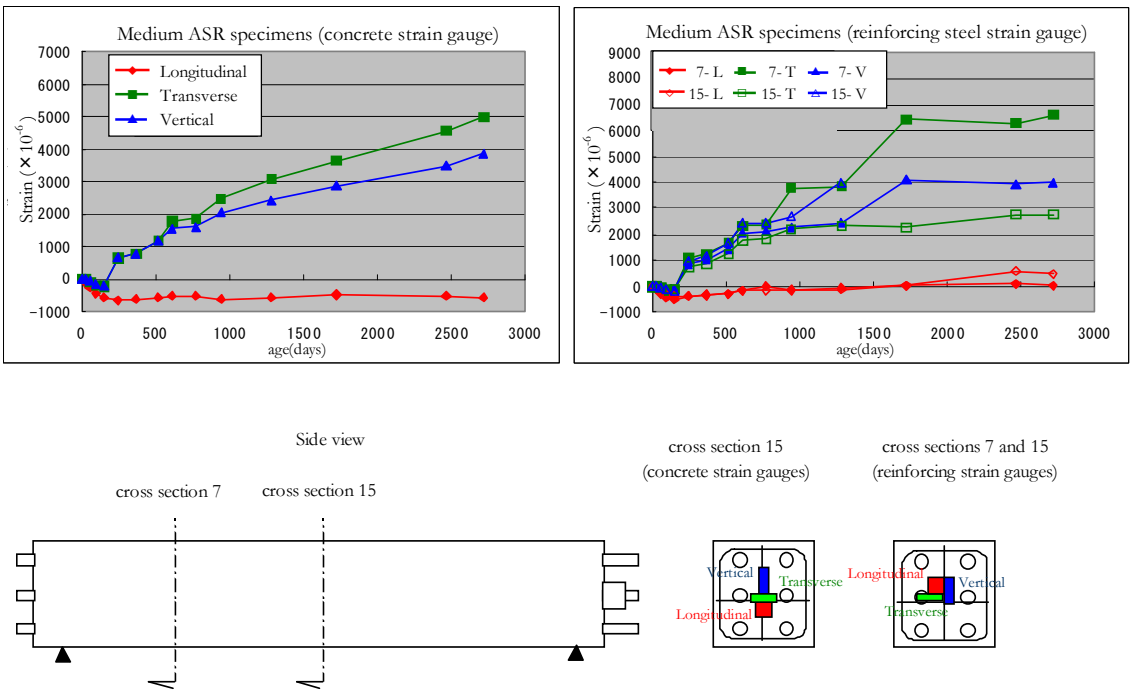

FIGURE 6: Changes in concrete internal strain in the medium ASR specimen

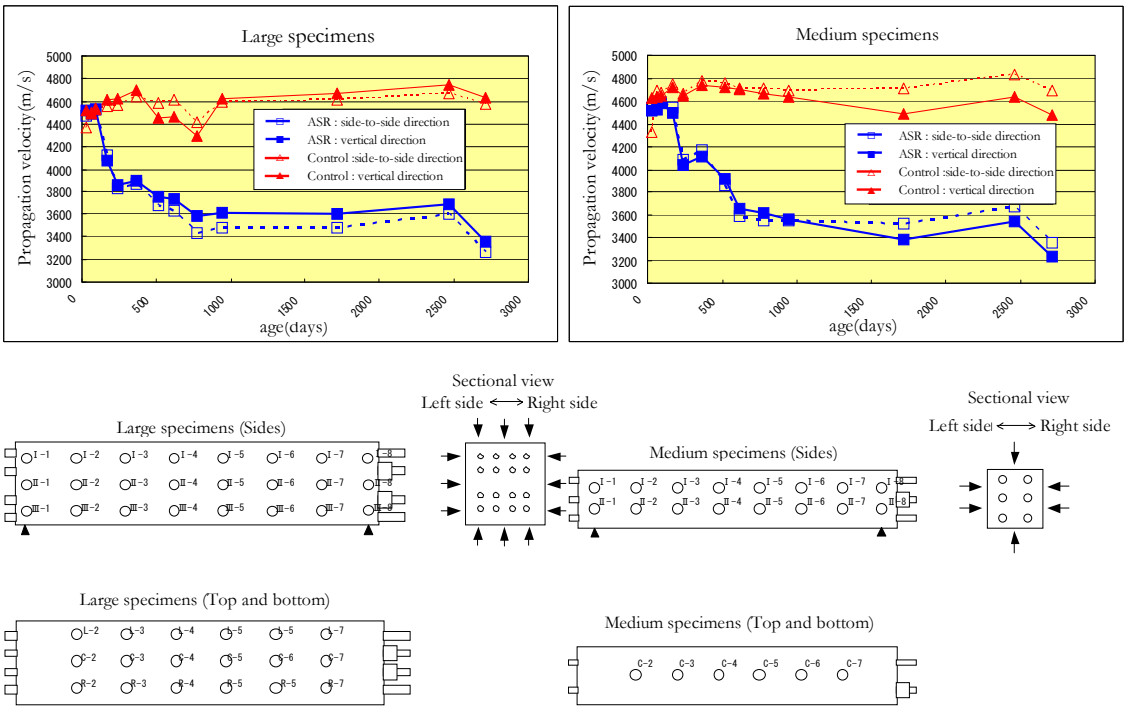

FIGURE 7: Changes in ultrasonic propagation velocity

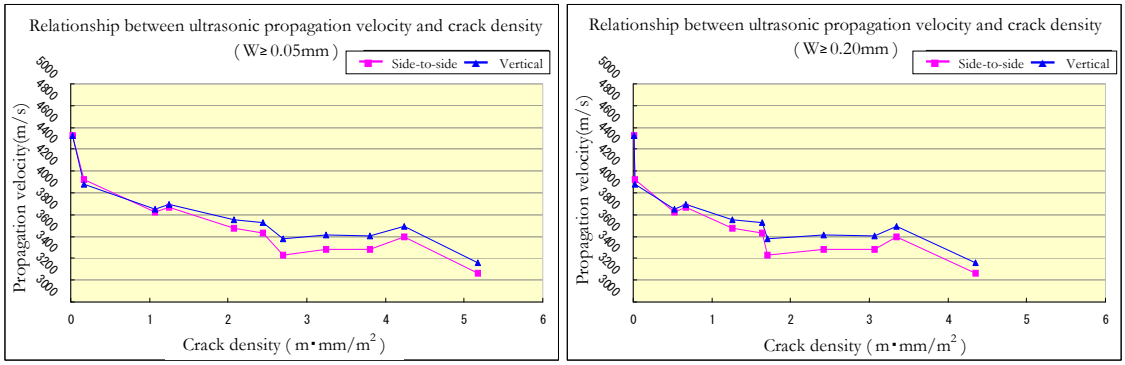

FIGURE 8: Ultrasonic propagation velocity vs. crack density in the large ASR specimen

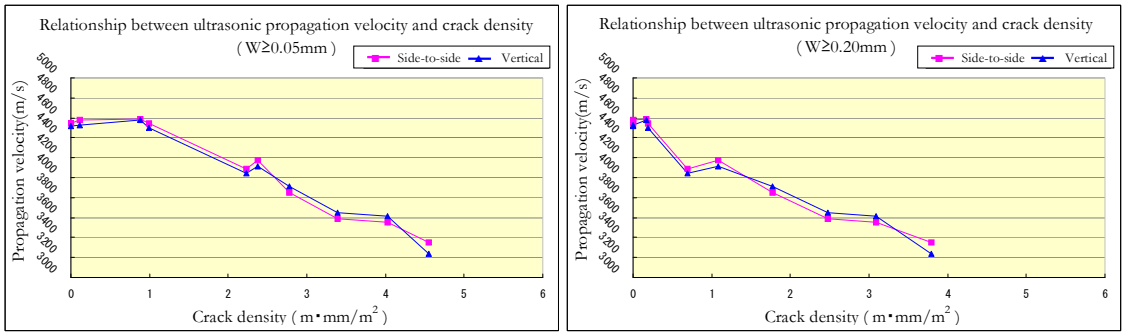

FIGURE 9: Ultrasonic propagation velocity vs. crack density in the medium ASR specimen

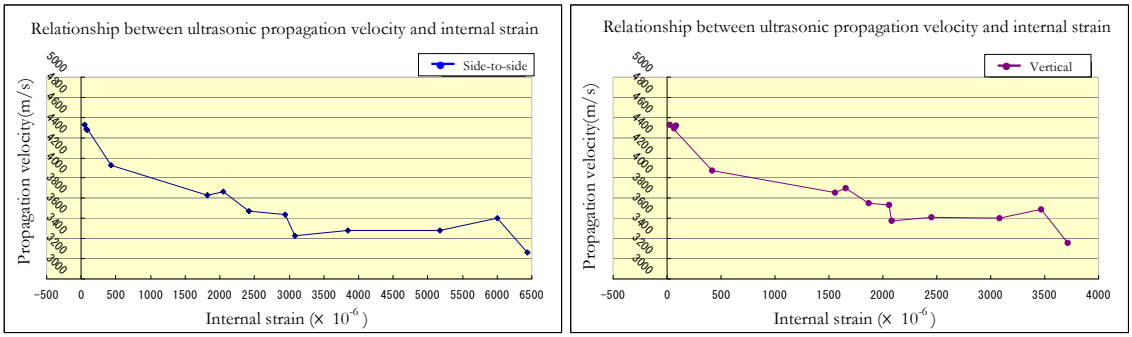

FIGURE 10: Ultrasonic propagation velocity vs. concrete internal strain in the large ASR specimen

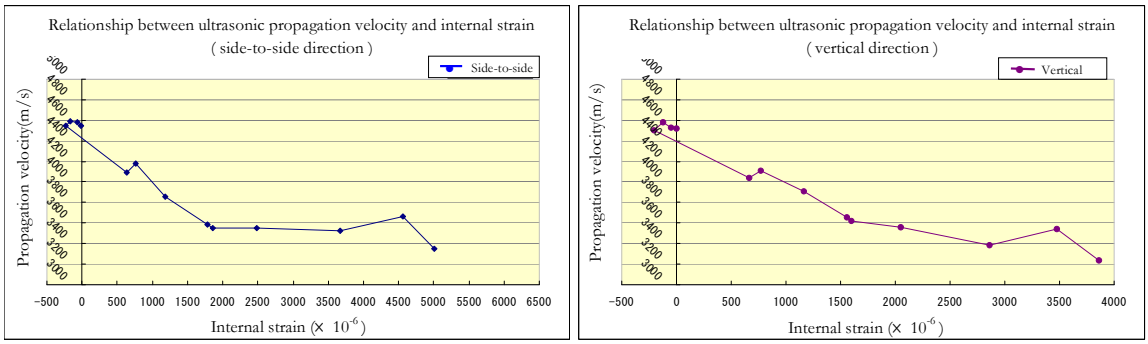

FIGURE 11: Ultrasonic propagation velocity vs. concrete internal strain in the medium ASR specimen

FIGURE 12: View of the loading test

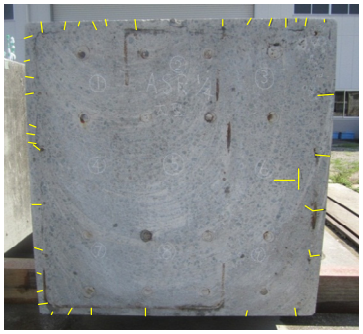

FIGURE 15: Crack distribution in a cut section (Large ASR specimen)

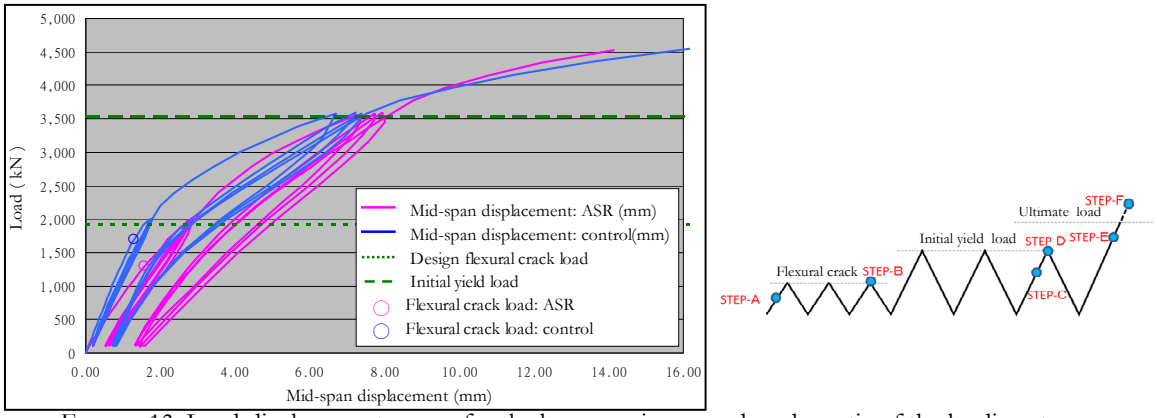

FIGURE 13: Load-displacement curves for the large specimens and a schematic of the loading steps

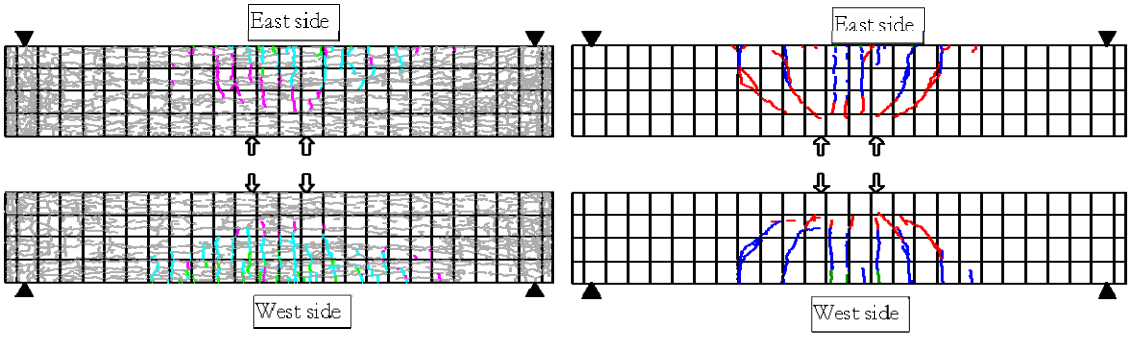

Large ASR specimen Large control specimen

FIGURE 14: Flexural cracks

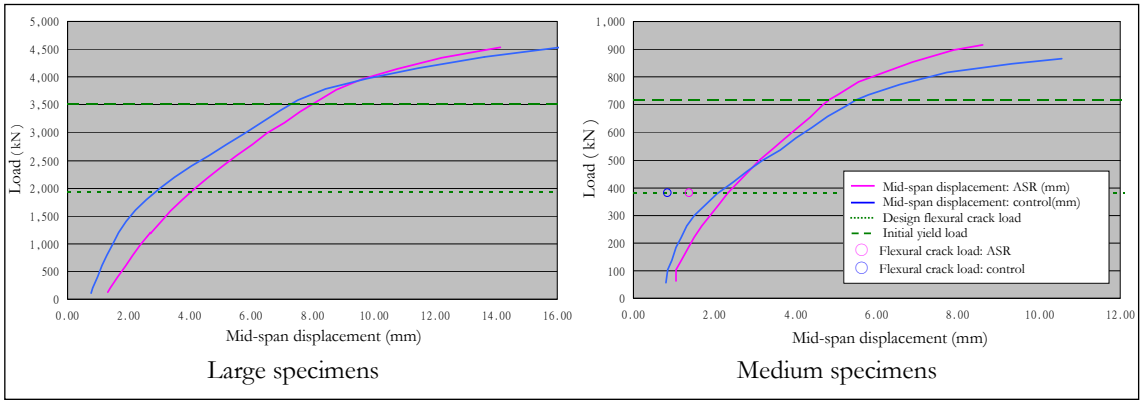

Large specimens Medium specimens

FIGURE 16: Load-displacement curves at the last loading step

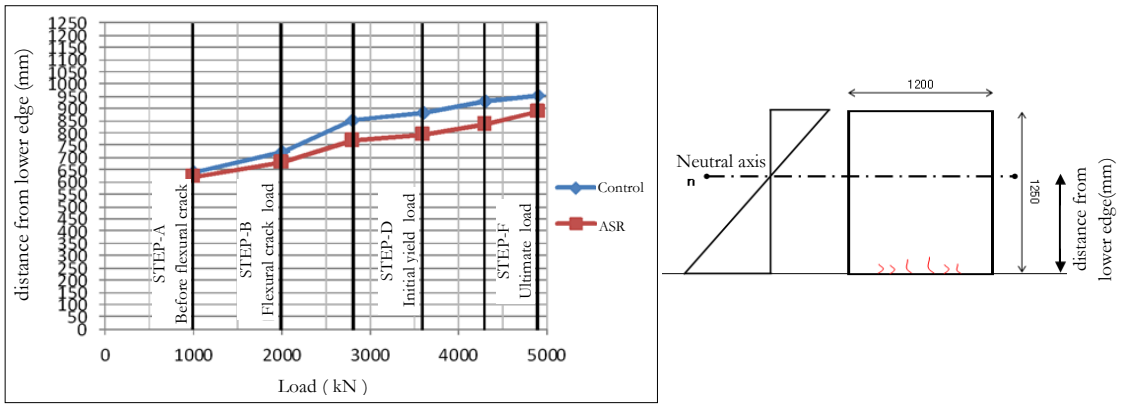

FIGURE 17: Changes in neutral axis in the large specimens

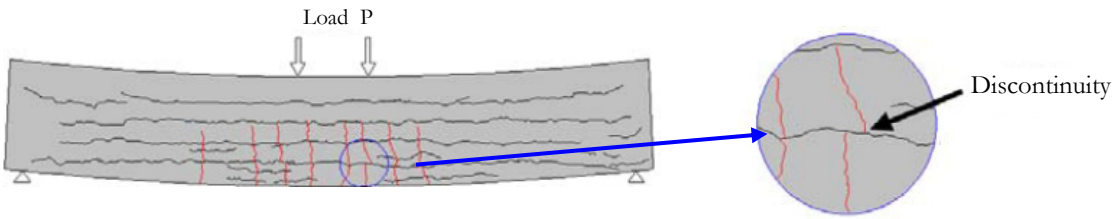

FIGURE 18: Flexural cracks in an ASR-affected beam under load